Prepared for International Symposium on Correlation and Polarization in Electronic and Atomic Collisions

ALIGNMENT AND ORIENTATION IN ION-ATOM COLLISIONS*

M. Kimura
Argonne National Laboratory, Argonne, IL 60439, and
Department of Physics, Rice University, Houston, TX 77251

and

N. F. Lane
Department of Physics and Rice Quantum Institute, Rice University
Houston, TX 77251

ABSTRACT

Recent progress in the theoretical study of alignment and orientation in atom-atom and ion-atom collisions at intermediate energies is reviewed. Recent systematic studies of the alignment and orientation of electronic charge cloud distributions of excited states resulting from such collisions clearly have provided more detailed information about the underlying collision dynamics. However, since accurate determination of these parameters is quite difficult, both theoretically and experimentally, a close collaboration between theory and experiment is necessary for a deeper understanding of the collision dynamics. A more complete approach, where the full density matrix is determined, is also discussed.

---

*Work supported by the U.S. Department of Energy, Office of Health and Environmental Research, under Contract W-31-109-Eng-38, and by the Office of Basic Energy Sciences.

1. INTRODUCTION

When energetic particles undergo a collision, the particles can experience elastic as well as inelastic events, namely, electronic excitation, charge transfer, and ionization. Because these collision events are often interrelated in a complex manner, it is quite difficult to obtain detailed knowledge about the underlying collision mechanisms.

Since the birth of the quantum mechanics, atomic physicists have devoted their efforts, both experimentally and theoretically, to the determination of accurate cross sections for inelastic scattering processes and to the qualitative understanding of collision dynamics responsible for these processes; such studies are likely to continue for the forseeable future. Only recently, however, have researchers begun to make progress at a more fundamental level by addressing the questions: "When and how do inelastic events take place during collisions, how do they depend on various collision parameters, and how do the electrons behave during such events?" Answers to these important questions will require intimate collaborative studies involving experiment and theory. Some such experimental and theoretical efforts have been successful in the last few years.

Recent advances in experimental technique have made possible systematic determinations of the orientation and alignment of electronic charge cloud distributions of excited states resulting from collisions of ions and atoms with atomic and molecular targets.[1-3] By making such measurements at selected well-defined scattering angles, it is possible to extract these parameters at specific impact parameters and thereby probe in more depth the true nature of the excitation and charge transfer mechanisms that control the collision process. A similar kind of experiment is the measurement of properties of photons produced in charge transfer and excitation collisions. The observed intensity and polarization of photons are analyzed in terms of a density matrix, elements of which are directly related to the electric dipole moment of the excited state formed in the collision.[4-6] This knowledge also elucidates precise collision

mechanisms for a variety of inelastic events in atomic collisions. In theoretical treatments of the orientation and alignment parameters, the results are often very sensitive to approximations made in the calculation and to various collision parameters (e.g., velocity and impact parameter) that define the conditions of the collision.[7] Hence extreme care is required in choosing the best theoretical approach to deal with a specific problem. Conversely, comparisons of the type described above can be sensitive measures of the validity of a theoretical method.

In this paper, we will review the current understanding of the general problem in the context of specific one- and two-electron systems.

2. THEORY

The theoretical approach appropriate to the range of energies considered in this work ($E \lesssim 25$ keV/amu) is the semiclassical impact parameter method in which the time-dependent Schrödinger equation is solved numerically for each impact parameter, energy, and initial internal electronic state of interest.[8] The excitation and charge transfer collision amplitudes are extracted from the "outgoing" asymptotic ($t \to +\infty$) form of the wavefunction, and from these amplitudes the orientation and alignment parameters and the cross sections are determined.

The time-dependent Schrödinger equation is solved by expanding the wavefunction in terms of a basis set of internal electronic-state functions. This basis may be of various forms, the most obvious being products of atomic-orbital (AO) functions or Born-Oppenheimer molecular-orbital (MO) functions.[9] Although some overlap exists where both AO and MO approaches may be applicable, the MO approach is considered to be more appropriate at lower energies and small impact parameters (close encounters). Hence, we adopt the latter in our treatment.

2.1 Molecular State

For simplicity, we restrict our discussion to one-electron (pseudo one-electron) systems. The generalization of the theory to many-electron systems is straightforward in principle. However, the jump from a one-electron system to a two-electron system is numerically large and requires an enormous amount of additional computer time to produce the necessary molecular states. This is largely due to the exponential increase in the number of molecular integrals that must be evaluated.

One-electron configuration interaction structure calculations were performed to obtain the molecular wavefunctions and energies. Pseudopotentials[10] were used to represent the inactive electrons. Within the Born-Oppenheimer approximation, the calculation of the eigenvalues reduces to determining the solution of the one-electron Schrödinger equation. (Atomic units are used throughout.)

$$\left[-\frac{1}{2}\vec{\nabla}_r^2 + V_A(\vec{r}_A) + V_B(\vec{r}_B) + V_{AB}(R) - E_i(R)\right]\phi_i^{MO}(\vec{r}, R) = 0 \quad . \tag{1}$$

where $\vec{r}_A$ is the position vector of the single active electron with respect to the A atom, and $\vec{r}_B$ represents the electron with respect to the B atom. Correspondingly, $V_A(\vec{r}_A)$ and $V_B(\vec{r}_B)$ are the effective interactive potentials between the electron and the A atom and the B atom, respectively. $V_{AB}(R)$ is the potential that approximates the interaction between cores.

The ℓ-dependent pseudopotentials $V_A(\vec{r}_A)$ and $V_B(\vec{r}_B)$ for the interaction of the electron with X = A or B are given in the general case by

$$V_x(\vec{r}_x) = \sum_{\ell=0}^{\infty} \sum_{m=-\ell}^{\ell} V_x(r_x) \left| Y_{\ell m}(\hat{r}_x) \right\rangle \left\langle Y_{\ell m}(\hat{r}_x) \right| \tag{2}$$

with

$$V_x(r_x) = a_{x\ell}\exp(-b_{x\ell}r^2) - \frac{Z_x}{r_x} - \frac{\alpha_{xd}}{2(r_x^2 + d_x^2)^2}$$

$$- \frac{\alpha_{xq}}{2(r_x^2 + d_x^2)^3} \quad . \tag{3}$$

The Gaussian parameters a_ℓ and b_ℓ are usually determined by iterative fits to spectroscopic data. The parameter Z_x is the charge of the core as seen by the electron at large distances, and α_d and α_q are the dipole and quadrupole polarizabilities, respectively. The cutoff parameter d serves to limit the range of the dipole and quadrupole forces to the region outside the core.

2.2 Coupled Equations

Assuming that the nuclear motion is described classically by $\vec{R}(t)$, we solve the resulting time-dependent Schrödinger equation for the electron. The state vector is expanded in an electron-translation-factor- (ETF-) modified molecular state set,[11]

$$\psi(\vec{r}, t) = \sum_i a_i(t)\, \phi_i^{MO}(\vec{r}, R(t)) \exp\left(\frac{1}{2}\vec{v} \cdot \vec{r}\, f_n(\vec{r}, R)\right) \quad , \tag{4}$$

where $f_n(\vec{r}, R)$ is the switching function, which incorporates a molecular nature in the ETF and is required to approach ± 1 asymptotically ($R \to \infty$), depending upon the site to which an electron attaches itself. The ϕ_i^{MO} are the usual Born-Oppenheimer states, which satisfy Eq. (1) and are obtained by the method described in Section 2.1. Substitution of Eq. (4) into the time-dependent Schrödinger equation yields the first-order, linear, coupled equations, according to the standard procedure:[12]

$$i\dot{a}_i = E_i a_i + \sum_j \vec{v} \cdot (\vec{P} + \vec{A})_{ij}\, a_j \quad , \tag{5}$$

where

$$P_{ij} = \langle \phi_i^{MO} | -i\vec{\nabla}_R | \phi_j^{MO} \rangle \tag{6a}$$

$$A_{ij} = i \langle \phi_i^{MO} | [H_{e\ell}, \frac{1}{2} f_j \vec{r}] | \phi_j^{MO} \rangle \quad , \tag{6b}$$

where $H_{e\ell}$ is the electronic Hamiltonian described in Eq. (1).

The matrix element P_{ij} is designated as the nonadiabatic coupling; A_{ij} represents the ETF correction. We have adopted a switching function of the form

$$f_i(\vec{r}, R) = \tanh[R\beta\eta] \quad , \tag{7}$$

where β is a parameter and η is the "angular" spheroidal coordinate. The parameter β was determined to minimize the sum of the squares of the ETF-corrected nonadiabatic coupling matrix elements to certain excited states.[12] In a rotating coordinate frame, Eqs. (6a, 6b) are made up of two distinct contributions, radial and rotational coupling and their corresponding ETF corrections. Equation (5) is solved numerically to obtain the scattering amplitude for various channels, subject to appropriate initial conditions. The square of the scattering amplitude gives the transition probability for a selected channel of interest at a specific collision energy and impact parameter. Straight-line trajectories were employed for the heavy particles.

2.3 Polarization Parameters[13,14]

The electronic charge cloud of an excited atom or ion after a collision not only changes size; it also changes shape and rotates. It can be characterized by coherence parameters; for P states, two parameters, the alignment angle γ relative to the scattering angle and inherent angular momentum (orientation) $\langle L_\perp \rangle$ as defined in Fig. 1, are significant. The parameters for the electron cloud for the ^2P state are defined in terms of three Stokes parameters (P_1, P_2, P_3) as

$$\tan 2\gamma = \frac{P_2}{P_1} \tag{8a}$$

and

$$\langle L_\perp \rangle = -\frac{P_3}{P} \quad . \tag{8b}$$

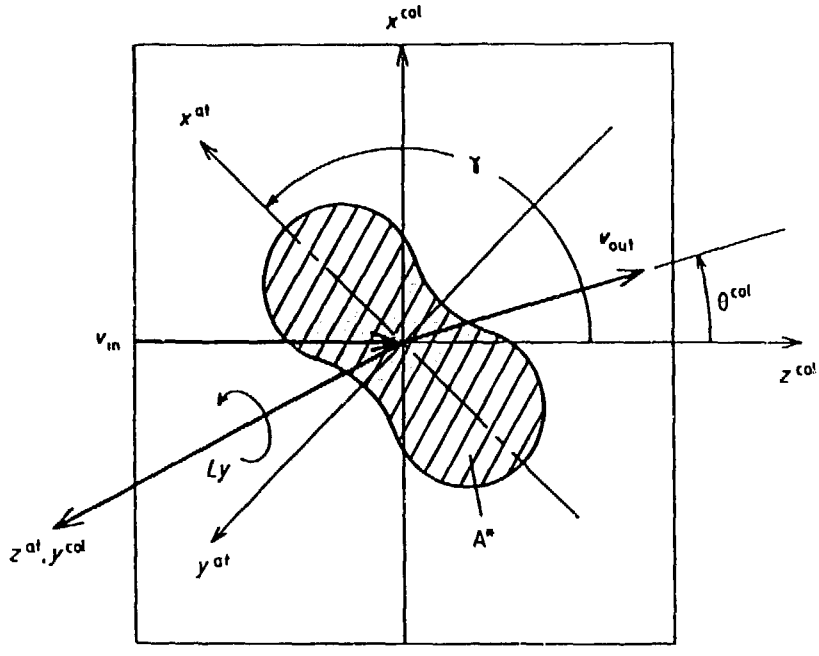

Fig. 1. Collision frame as defined by relative velocity before (v_i) and after (v_{out}) collision. The atomic charge cloud of A^*, its alignment angle γ and transferred angular momentum $\langle L_\perp \rangle$ are also shown (Ref. 2).

The Stokes parameters are defined by the scattering amplitudes as

$$P_1 = 2\lambda - 1 \quad , \tag{9a}$$

$$P_2 = -\, 2\sqrt{\lambda(1-\lambda)}\,\cos\chi \quad , \tag{9b}$$

$$P_3 = 2\sqrt{\lambda(1-\lambda)}\,\sin\chi \quad , \tag{9c}$$

$$P = P_1 + P_2 + P_3 \quad , \tag{9d}$$

where λ and χ are an amplitude ratio and phase difference given as

$$\lambda = \frac{|a_\sigma|^2}{|a_\sigma|^2 + |a_\pi|^2} \quad , \tag{10a}$$

$$\chi = \arg \left|\frac{a_\pi}{a_\sigma}\right| \quad , \tag{10b}$$

and a_σ and a_π are the σ and π state asymptotic amplitudes, respectively. The integral alignment A_{20} is defined as

$$A_{20} = \frac{\sigma_1 - \sigma_0}{\sigma_0 + 2\sigma_1} \quad , \tag{11}$$

where σ_1 and σ_0 are the m-substate cross sections for $A(np_{\pm 1})$ and $A(np_0)$ excitation, respectively.

These parameters can also be described by using state multipoles (orientation vector and alignment tensor), which are closely related to the density matrix elements.[14] Since these representations are frequently used in the literature and provide a different perspective on the parameters, it is helpful to write explicit expressions for relevant processes. For n=2 excitation, the state multipoles are:

$$\langle T(00)^+_{00} \rangle = \sigma(2s) \quad , \tag{12a}$$

$$\langle T(11)^+_{00} \rangle = \frac{1}{\sqrt{3}}\, \sigma(2p) \quad , \tag{12b}$$

$$\langle T(11)^+_{11} \rangle = \frac{i}{\sqrt{3}}\, \mathrm{Im}\langle a_\sigma a^*_\pi \rangle \quad , \tag{12c}$$

$$\langle T(11)^+_{21} \rangle = -\sqrt{2}\, R_e\langle a_\sigma a^*_\pi \rangle \quad , \tag{12d}$$

$$\langle T(11)^+_{20} \rangle = \sqrt{2}/3\, (|a_\pi|^2 - |a_\sigma|^2) \quad . \tag{12e}$$

In terms of three moments, the orientation is given by

$$\langle L_\perp \rangle = + i\sqrt{2}\, \frac{\langle T(11)^+_{11} \rangle}{\langle T(11)^+_{00} \rangle} \tag{13}$$

and the partial alignment (at one impact parameter) by

$$A'_{20} = \sqrt{2}\,\frac{\langle T(11)^{+}_{20}\rangle}{\langle T(11)^{+}_{00}\rangle} \quad . \tag{14}$$

Eqs. (13) and (14) are equivalent, apart from some constant factors, to Eqs. (8b) and (11). In any representation, the important observables are the orientation and alignment parameters.

As an illustration of the development of electronic charge distribution during an ion-atom collision, Fig. 2a shows contour plots at several times of the square of the time-dependent electronic wavefunction of the He^{++}/H system at an impact energy of 1 keV and impact parameter of 0.53 a_0.[15] Also shown in Fig. 2a are the adiabatic potential curves for the He^{++}/H system. The collision dynamics are dominated by the rotational coupling between the $2p\sigma$ (the initial channel of He^{++} on H) and $2p\pi$ states, which are degenerate in the united-atom limit. Thus, the final state of the system evolves toward a superposition of states corresponding to a 1s electron on H (with a somewhat reduced probability with respect to the initial distribution) and a $2p_m$ ($m = \pm 1$) electron on He^{+}. The principal axis of the latter charge distribution, resulting from charge transfer, is essentially perpendicular to the internuclear axis, so that the alignment is approximately 90° (plus the scattering angle). Since there is very little mixing of the $2p_0$ ($m=0$) state, the transferred angular momentum (orientation) is nearly zero (see Eq. 8b, 9c, and 10a,b). At larger impact parameters, the radial coupling between the $2p\sigma$ and $3d\sigma$ states plays an important role in producing significant charge transfer to the 2s and 2p ($m=0$) states of He^{+}. The density contours, shown in Fig. 2b for 8 keV and $b = 6.11\ a_0$, reflect this state mixing.

3. COLLISIONS OF H ATOMS WITH He ATOMS[16]

The two electrons in the He atom are tightly bound and thus are assumed to be only slightly perturbed during the collision, while the electron in the H atom is loosely bound and is assumed to be actively involved in the actual collision dynamics. Hence, a reasonable approximation is to treat the system as a pseudo-one-electron-

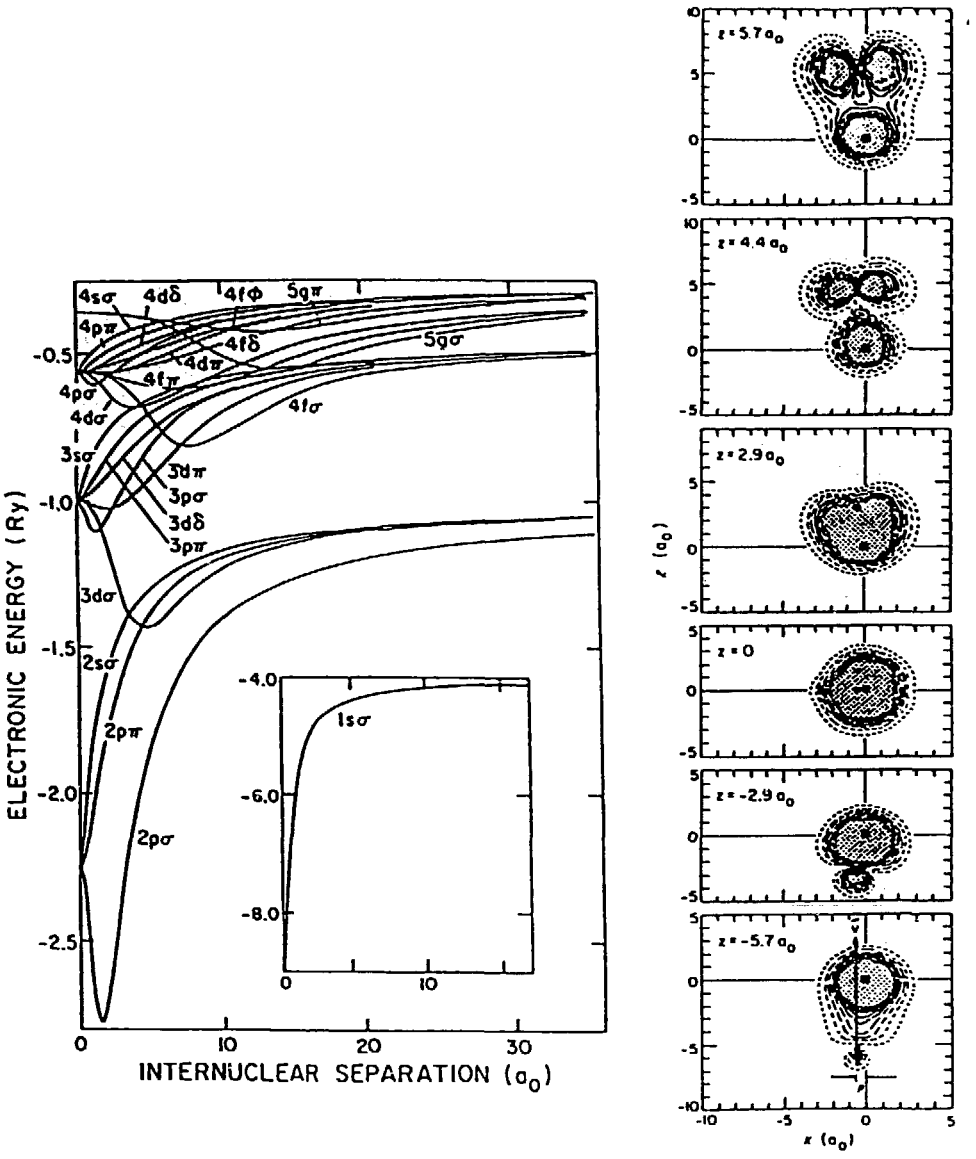

Fig. 2a. Adiabatic potential curves of the He^{++}/H system and contour plots of electron charge density in the collision plane (Ref. 15). Charge transfer at impact parameter 0.53 a_0 and energy 1 keV.

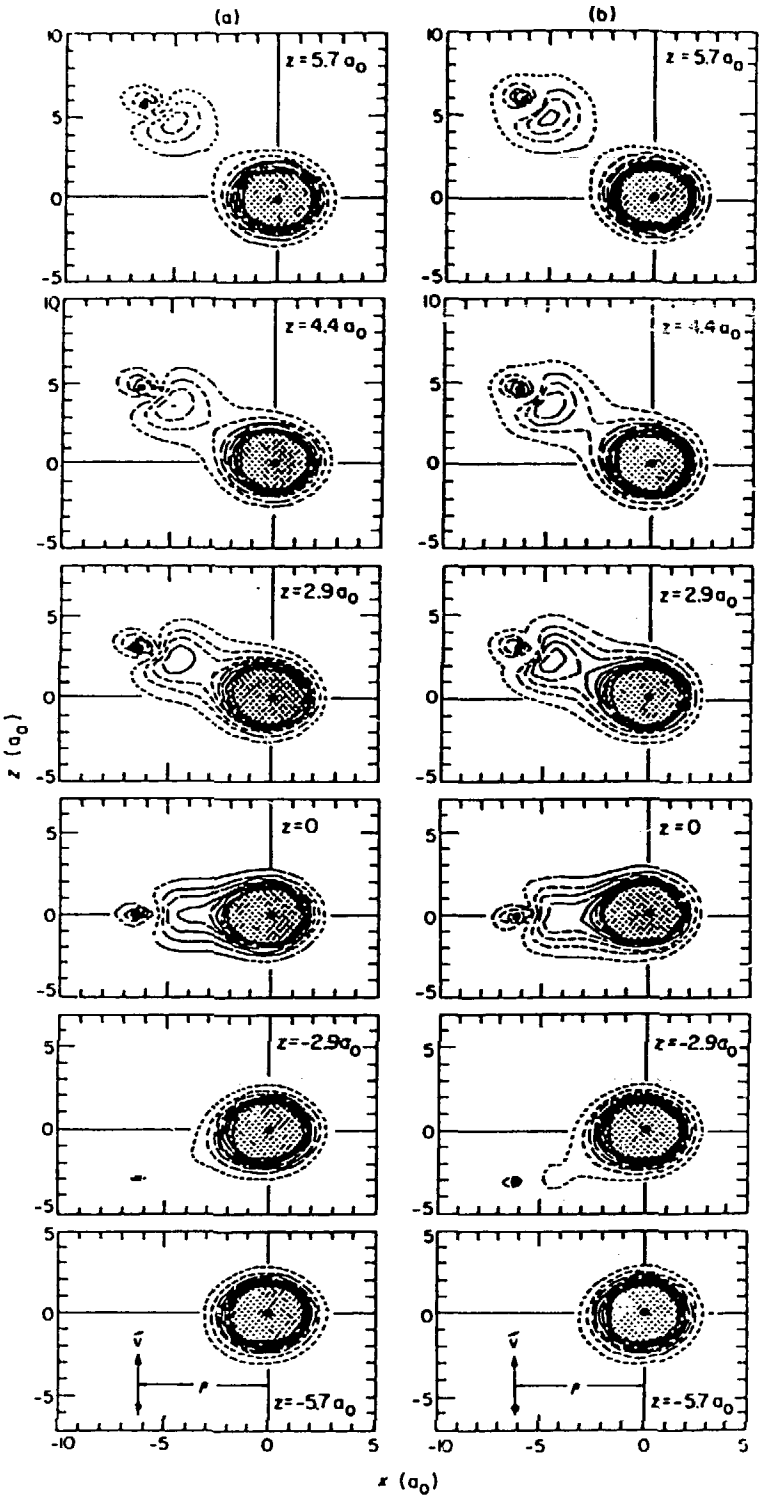

Fig. 2b. Charge transfer at impact parameter 6.11 a_0 and energy 8 keV. (a) 22-MO without the ETF; (b) 10-MO with the ETF.

collision system. By using a pseudopotential representation of the electron-He interaction, we obtained the adiabatic potential energies for the He/H system shown in Fig. 3a. The $^2\Sigma$ (solid curves) and the $^2\Pi$ (dashed curves) molecular states are shown. The schematic (diabatic) molecular correlation diagram of the system is shown in Fig. 3b.

A general feature of the potential energies is the occurrence of strong mixing between the 1Σ and 2Σ molecular configurations for $R \lesssim 0.5\ a_0$. This is because the 1Σ and 2Σ configurations correlate with the $Li(1s^2 2p)$ and $Li(1s^2 2s)$ atomic states in the united-atom limit, as is seen in Fig. 3b. This curve-crossing at $R \approx 0.5\ a_0$, correlates with flux promotion during the incoming part of the collision. However, flux given to the 2Σ configuration will be redistributed by additional strong radial and rotational couplings within the H(n=2) manifold. The 1Σ and 1Π configurations are degenerate in the united atom limit, coinciding with the $Li(1s^2 2p)$ atomic level (see Fig. 3b). Thus, one expects a relatively strong rotational coupling between these states at small R. The 2Σ and 1Π configurations are almost identical except for the small R region ($\lesssim 1.5\ a_0$); outside this region, the corresponding rotational coupling might be expected to cause some flux redistribution within the H(n=2) manifold.

The behavior exhibited by the adiabatic energy curves is borne out by the radial coupling matrix elements. The important coupling terms between the ground and H(n=2) levels are shown in Fig. 4. The calculations indicate strong radial coupling between the 1Σ and 2Σ states that peaks at $R \approx 0.2\ a_0$. Other radial couplings involving the ground 1Σ state are relatively weak at all internuclear separations. The radial coupling between the 2Σ and 3Σ states possesses a long-range tail extending beyond $R \approx 5\ a_0$. This tail may be related to flux redistribution in the outgoing part of collision. The rotational coupling between the 1Σ and 1Π states is of secondary importance.

A collision history in Fig. 5 shows excitation probabilities as functions of collision time and clearly indicates that the Π state

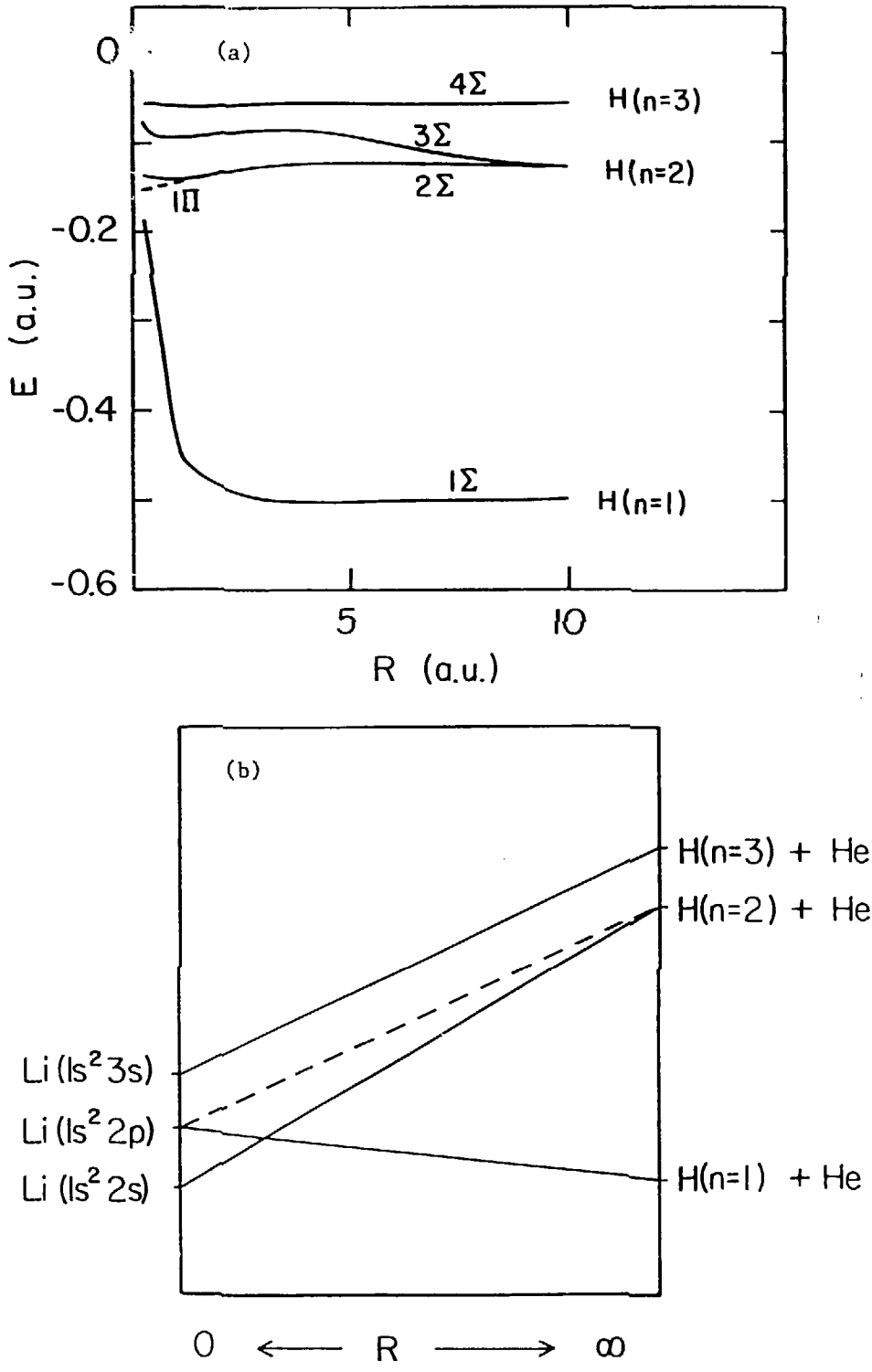

Fig. 3. Collision of H with He. (a) Adiabatic potential energies. (b) Diabatic molecular correlation diagram.

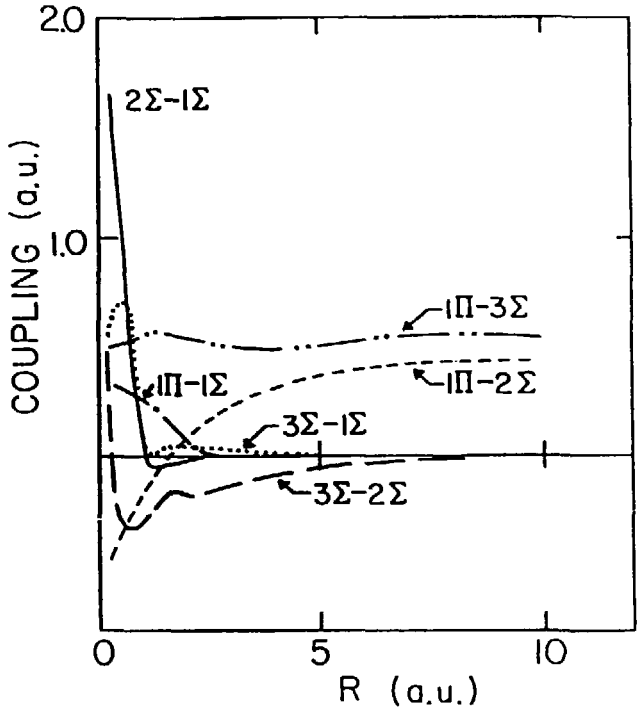

Fig. 4. Coupling terms between ground and H(n=2) levels for collision of H with He.

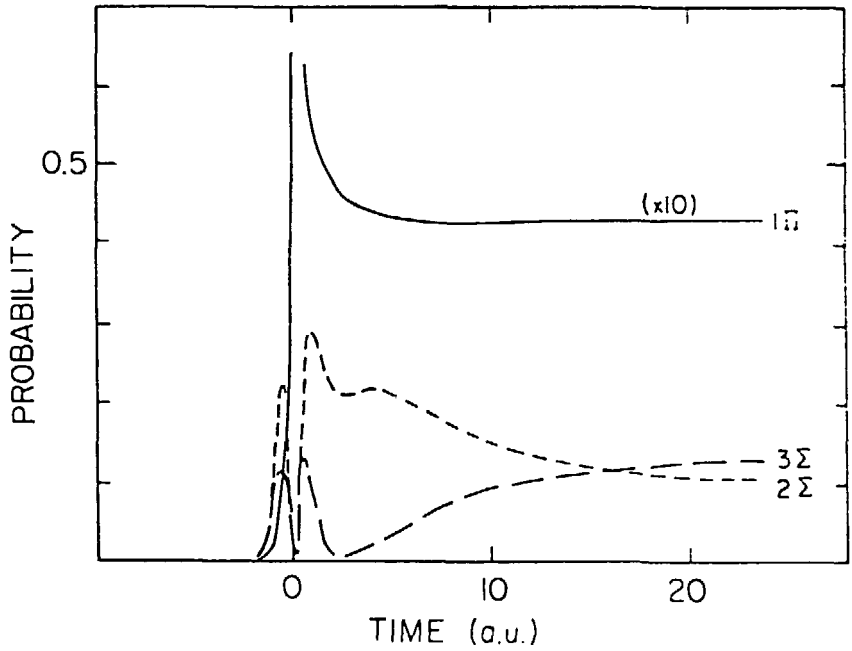

Fig. 5. Change in excitation probabilities with time for collision of H with He at impact parameter 0.2 a_0 and energy 4 keV.

couples with the Σ states only at small R, and soon completely decouples. The 2Σ and 3Σ states continue to couple with one another until quite large internuclear separations are achieved, and therefore contribute significantly to the redistribution of flux between the H(2s) and H(2p) states. As the impact parameter is increased, flux promotion to the excited Π-state through 1Σ-1Π rotational coupling quickly disappears, as is apparent from the coupling shown in Fig. 4. However, certain general features of the coupling scheme (namely, short-range 1Σ-1Π coupling and long-range 2Σ-1Π, 3Σ-1Π, and 2Σ-3Σ coupling) remain unchanged for a particular collision energy and impact parameter.

The present integral [integrated over the impact parameter; see Eq. (11)] alignment A_{20} values for the excited H(2p) states are shown in Fig. 6 along with the Bielefeld measurement of Hippler et al.[17] The negative values observed for A_{20} indicate that excitation to the $H(2p_0)$ level is overwhelmingly the dominant process; theoretically, this is found to occur through the strong 1Σ-2Σ radial coupling in this energy regime. The lack of any prominent structure in the A_{20} measurements also indicates very little interference from other types of coupling. From a theoretical perspective, the presence of important simultaneous couplings generally leads to oscillations between two corresponding states at amplitudes that are related to collision energy. The small variation of A_{20} with respect to collision energy can be explained in terms of the dominance of a single strong radial coupling mechanism. A similar energy dependence of A_{20} is found for the system H on Ne and Ar targets, both experimentally[17] and theoretically.[18] Since the general nature of the adiabatic potential curves is qualitatively quite similar for all three systems, the observed similarity in A_{20} values is not surprising.

The calculated transferred angular momentum $\langle L_\perp \rangle$ (orientation) perpendicular to the scattering plane is depicted in Fig. 7 as a function impact parameter for the two energies 1.0 and 1.5 keV, along with the experimental results of Hippler et al.[17] Agreement between

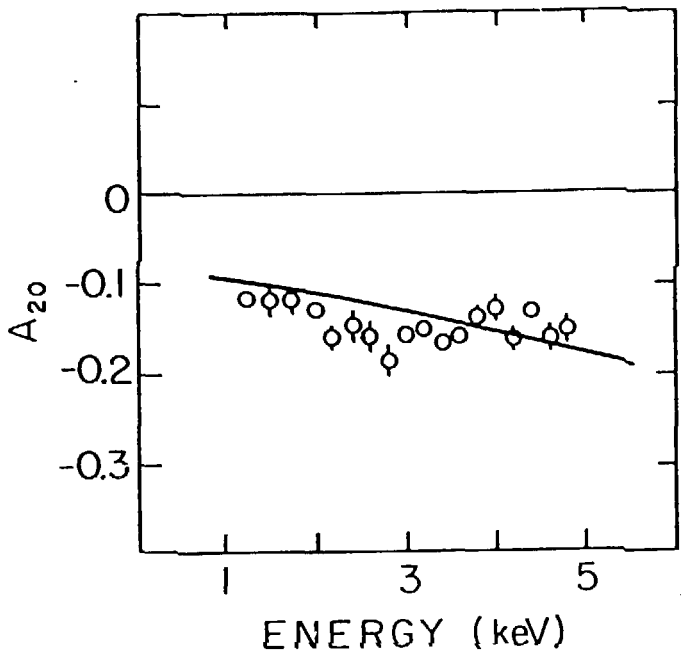

Fig. 6. Alignment A_{20} values (integrated over impact parameter) for excited H(2p) states in collision of H with He. ——, calculated values (Ref. 16); o, experimental results (Ref. 17).

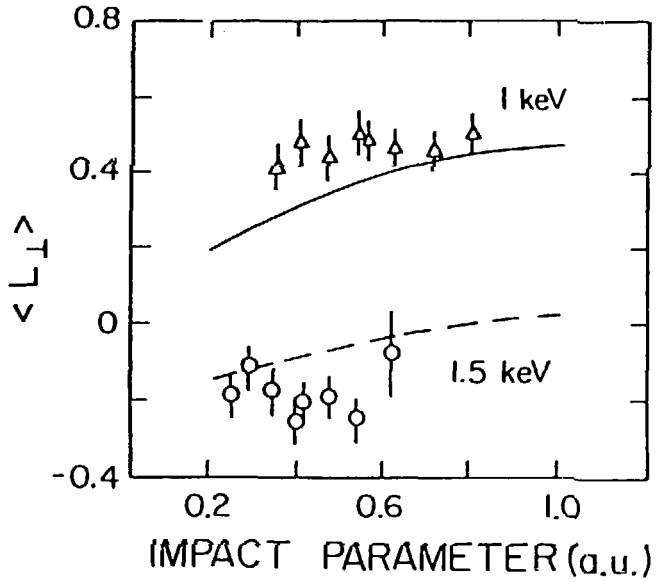

Fig. 7. Orientation perpendicular to scattering plane as a function of impact parameter for collision of H with He. - - - and ——, calculated values (Ref. 16); o and Δ, experimental results (Ref. 17).

the present theory and the experiment is reasonably good. Neither the theoretical nor the experimental curves shows any notable structure except for a slightly increasing trend of the calculated angular momentum $\langle L_\perp \rangle$ at larger b, and a relatively strong energy dependence. The factor before the phase χ in Eq. (9c) has a relatively weak dependence on b. However, the relative phase χ of the excitation amplitudes for the $H(2p_0)$ and $H(2p_1)$ sub-levels is sensitive to the collision energy. This sensitivity gives rise to the strong energy dependence of the angular momentum, which, in turn, reflects the strength and the "attractive" or "repulsive" nature of the interaction potential experienced by the electron cloud, corresponding to positive or negative values of $\langle L_\perp \rangle$, respectively. This interpretation of our finding is in good qualitative agreement with the "rolling ball" model proposed by Hertel[2] and the "propensity rule" of Andersen.[3]

4. COLLISIONS OF Li^+ IONS WITH He ATOMS[7,19]

The recent theoretical interest[7,19,20] in the Li^+/He system was stimulated by the beautiful measurements of the Aarhus group.[19,21] Orientation and alignment parameters for the final states [Li(2p) and Li(3d)] resulting from charge transfer, and for $He(2^1P)$, resulting from excitation, have been reported by Andersen et al.[21] Since the experimental alignment and orientation studies have been performed at very small impact parameters, between 0.2 and 1.1 a.u. in the energy range from 1 to 25 keV, very precise molecular states at small internuclear separation ($R < 2$ a.u.) as well as a reasonably good representation of the molecular ETF might well be indispensable for an accurate description of the observed phenomena. Hence, the problem is *particularly well suited to testing by various theoretical approaches.*

Figures 8a and 8b illustrate adiabatic potential curves[7] and the corresponding diabatic MO diagram for the Li^+/He system. Important radial and rotational coupling regions are indicated by circles and rectangles, respectively (Fig. 8b), along with corresponding relevant internuclear distances. Figure 9 shows representative couplings. The

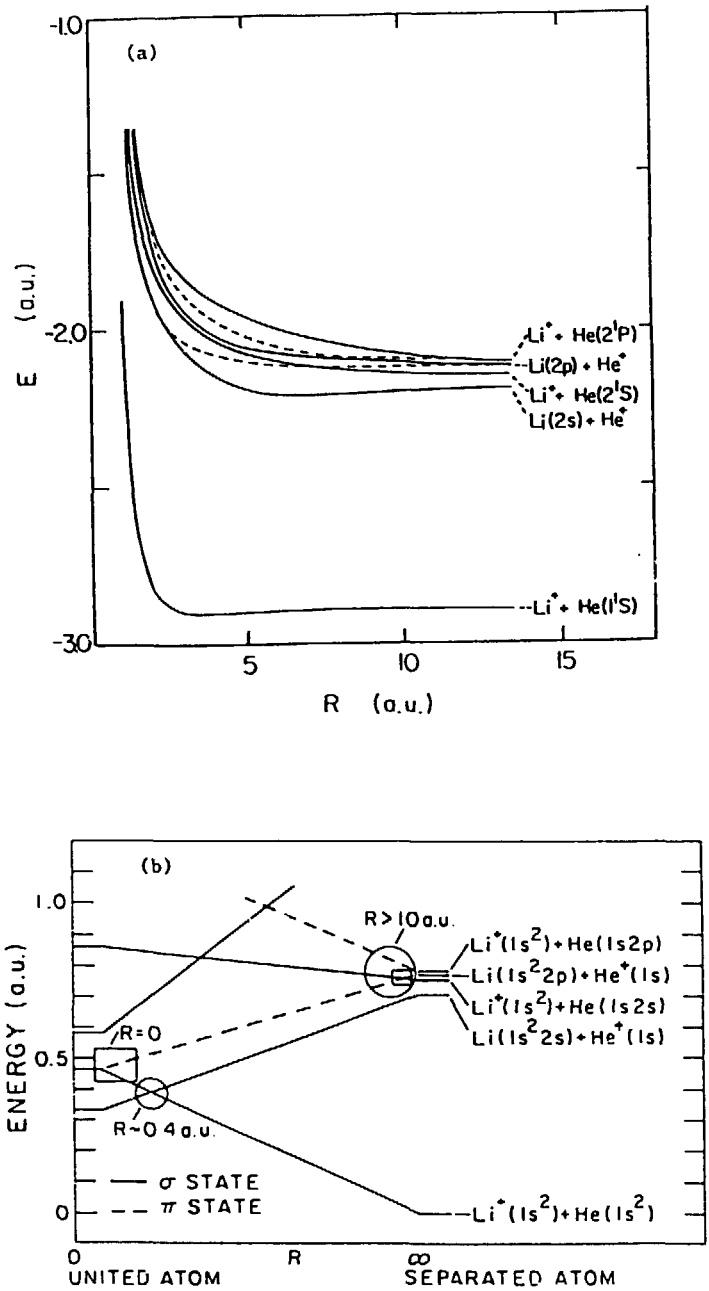

Fig. 8. Collision of Li^+ ion with He atom. (a) Adiabatic potential curves. (b) Diabatic molecular correlation diagram. Circles indicate radial coupling regions; rectangles indicate rotational coupling regions.

diabatic picture (Fig. 8b) along with the couplings in Fig. 9, indicates that the flux initially in the 2pσ ground state is promoted to the 2pπ state, which becomes degenerate with the ground state at the united-atom limit, through the strong 2pσ–2pπ rotational coupling. The narrow avoided crossing between the 2pσ and 2sσ states at R ~ 0.42 a_0 may also result in some flux promotion. However, as was pointed out by Sidis et al.[22] and shown also by Wahnon et al.,[20] the radial coupling between these states is rather weak; hence, the flux transfer to higher levels at this crossing should be small. The long-range π–π radial coupling between the $Li(2^2P_{\pm1})$ + He^+ and Li^+ + $He(2^1P_{\pm})$ states at larger R plays an extremely important role in the flux redistribution between these states. Correspondingly, the rotational coupling between asymptotically degenerate states on the same atom also plays some part in the flux redistribution. Of course, these two coupling mechanisms are important only for the exit channel in the collision. In this calculation, two-electron processes have

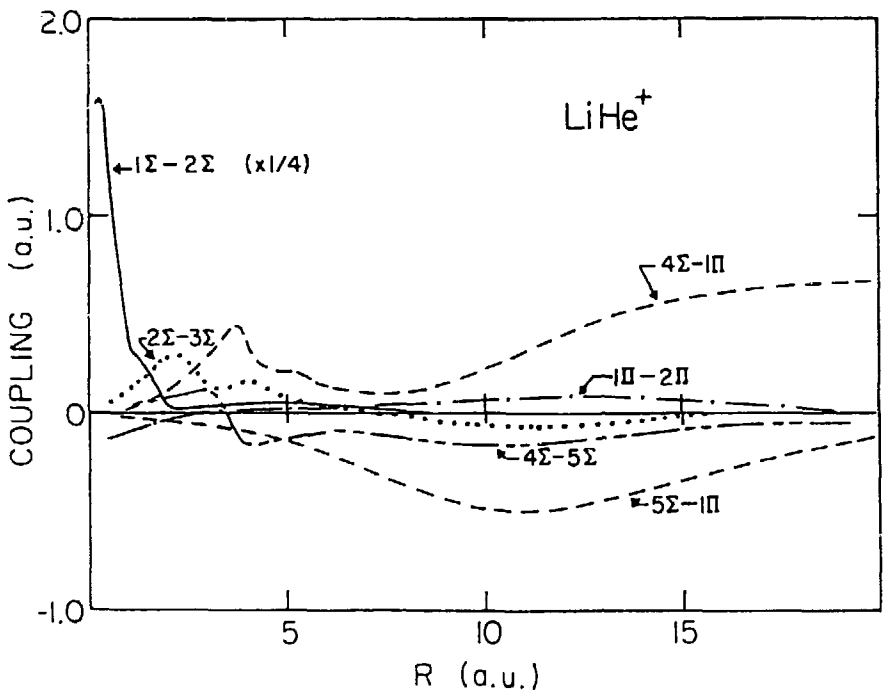

Fig. 9. Coupling terms for collision of Li^+ with He.

been assumed to be of negligible importance.

Our theoretical alignment angles γ_{Li} and γ_{He}, calculated by using the molecular ETF and the atomic ETF, are shown as functions of collision energy in Figs. 10a and 10b, respectively, along with the results of the experimental measurement of Andersen et al.[21] The calculations were performed for a single impact parameter b = 0.55 a_0, corresponding to the scattering angle selected in the measurements. The agreement between the present molecular-ETF calculation and the experimental results is satisfactory, while the calculation based on the atomic ETF agrees only in magnitude.

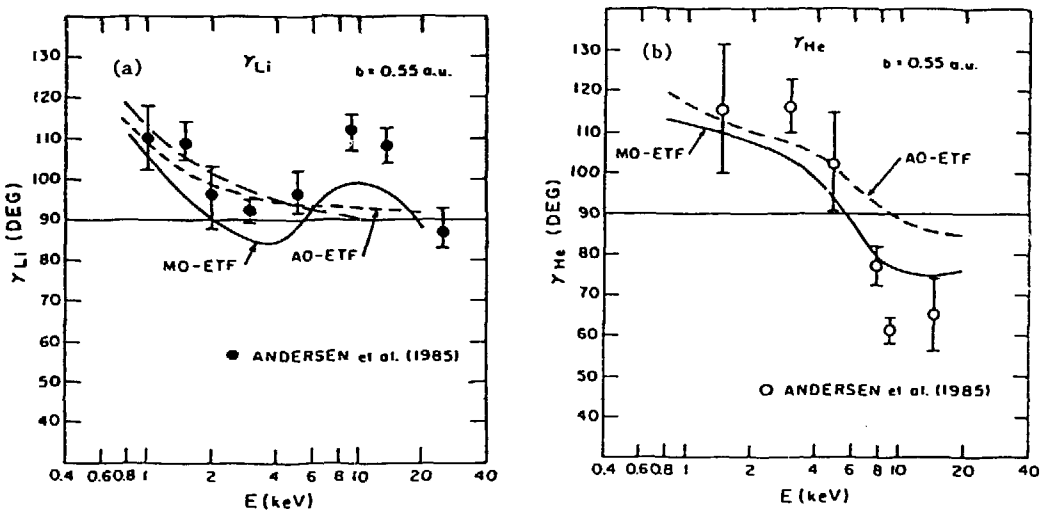

Fig. 10. Alignment angles for collision of Li^+ with He. Theoretical results (Ref. 7): ——, MO-ETF (optimized); - - - AO-ETF (plane wave). Experimental results (with error bars; Ref. 21): •, γ_{Li}, panel (a); o, γ_{He}, panel (b).

Wahnon et al.[20] have also studied the alignment and orientation of Li(2p) and He(2^1P) excited orbitals in the collision of Li^+ on He. Their treatment is similar to the one we adopted[7] except for the use of several simplifying assumptions, such as "half" collision method and the neglect of the ETF. Although their results are not in good quantitative agreement with the measurement,[21] they do reproduce some important features of the alignment and orientation parameters.

These comparisons strongly suggest that particularly for small impact parameter, such as $b \approx 0.55\ a_0$, optimized molecular ETF are necessary to correctly describe the electron translational motion in the two-center (molecular) field since small internuclear separations are involved; this clearly is reflected in the shape and magnitude of the corresponding coupling matrix elements. The atomic ETF treatment does not provide an accurate description of the collision dynamics in the region of small impact parameter. (See, for example, Ref. 11 for the ETF effect for a one-electron system.) This point is evident in the larger differences between the molecular ETF and the atomic ETF results shown in Fig. 10. These comparisons may provide an important additional contribution for the ETF dialogue that has been ongoing for many years.[11]

The oscillatory structure seen in the energy dependence of the alignment angle γ arises from the passage of the phase χ through π because of strong coupling between the two nearly degenerate channels that correlate to the Li(2^2P) + He^+ and Li^+ + He(2^1P) levels. Therefore, the probabilities for $2p\sigma$ and $2p\pi$ states corresponding to these two channels are strongly energy dependent. In the molecular picture, the charge transfer and excitation processes are closely related. When two ions and atoms approach sufficiently closely that they form a quasimolecule, they share the electron cloud. It follows that as the particles separate following the collision, the projectile has a maximum probability of having the electron distribution around it when the target has a minimum probability, and vice versa. Therefore, the probability of the charge transfer should be out-of-phase with that of the excitation. The out-of-phase oscillatory

structure in λ, the amplitude ratio, is somewhat more complex, since long range σ-π coupling is involved. The out-of-phase phenomena observed in the alignment angles γ_{Li} and γ_{He} (Fig. 10) correlates with that present χ and λ, and has the same physical base.

In Figs. 11a and 11b, the theoretical angular momentum (orientation) $\langle L_\perp \rangle$ of the electron cloud is plotted along with the measurement of Andersen et al. at b = 0.55 a_0[21] for Li and for He. Our theoretical results reproduce the experimental findings nicely. The calculated results for $\langle L_\perp \rangle$ vary monotonically from 0.39 at 0.8 keV to -0.80 at 25 keV, changing sign at about E ≈ 3.5 keV for Li. This indicates that the potential becomes effectively repulsive to the electron cloud as the collision energy increases. This result arises from the sign change of sin χ, and causes $\langle L_\perp \rangle$ to become negative at higher energies. A similar explanation can be given for the less satisfactory agreement observed for the atomic ETF calculation.[7] The remaining discrepancies observed between the theory and the experiment in the figures are perhaps due in part to inaccuracies in the MO wave function and ETF values and in part to experimental error.[21]

The study of the alignment and orientation in Li^+ + He collisions has been extended to include the excited electron cloud of the Li(3^2D) state at impact parameters between 0.2 and 1.1 a_0 and energies 2.5-15 keV.[19] Despite the use of a limited MO basis set for the calculation, the qualitative agreement obtained between the experimental and theoretical coherence parameters supports the appropriateness of the theoretical approach, i.e., the MO method with the MO-ETF. The study reveals that the main promotion mechanism for Li(3^2D) involves the $\Sigma \rightarrow \Pi \rightarrow \Delta$ two-step process. In contrast to the behavior of the alignment and orientation parameters for Li(2p) and He(2^1P) states. these parameters for the Li(3^2D) state show conspicuous oscillatory structures that are due mainly to interference effects associated with coupling of various intermediate states.

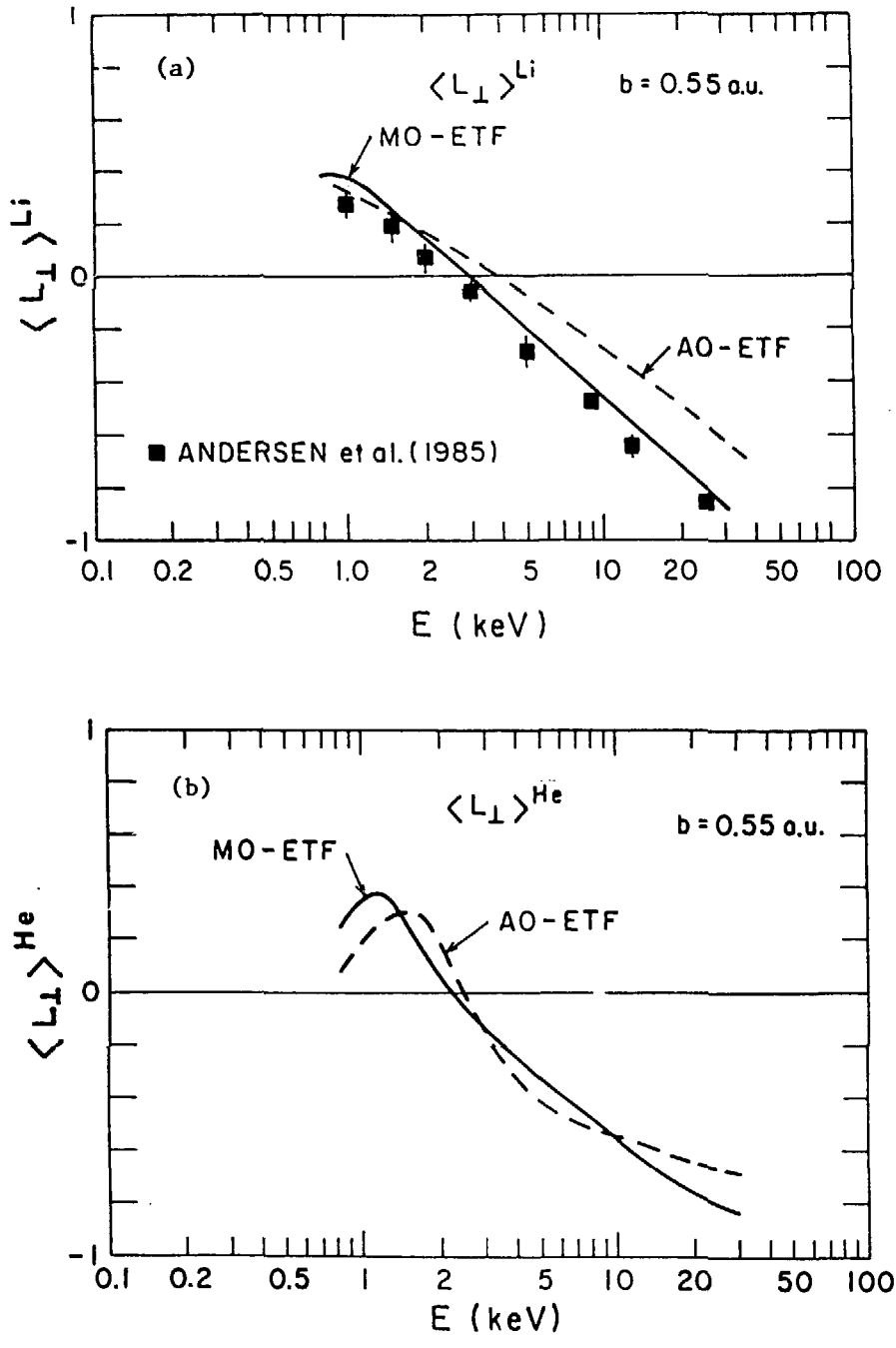

Fig. 11. Orientation of electron cloud for Li^+ (panel a) and He (panel b) at impact parameter 0.55 a_0. Theoretical results (Ref. 7): ——, MO-ETF (optimized); - - -, AO-ETF (plane wave). Experimental results (Ref. 21): .

5. COLLISIONS OF H^+ IONS WITH He ATOMS[23]

Since the H^+/He collision system is the simplest "complex" system and serves as the most fundamental prototype for a deeper understanding of the collision dynamics of more complex systems, a determined experimental effort has been made to determine the alignment and orientation parameters, as well as the density matrices for the H(n=2) and H(n=3) levels produced by charge transfer in H^+ + He collisions.[4-6,17] However, the experiment is extremely difficult particularly with regard to the detection of the H(n=3) level.[4-6] Thus, a closely coordinated collaborative effort between experiment and theory is required.[4-6,24]

Adiabatic potential curves and a schematic diabatic diagram for the H^+/He system are shown in Figs. 12a and 12b, respectively.[23,25]

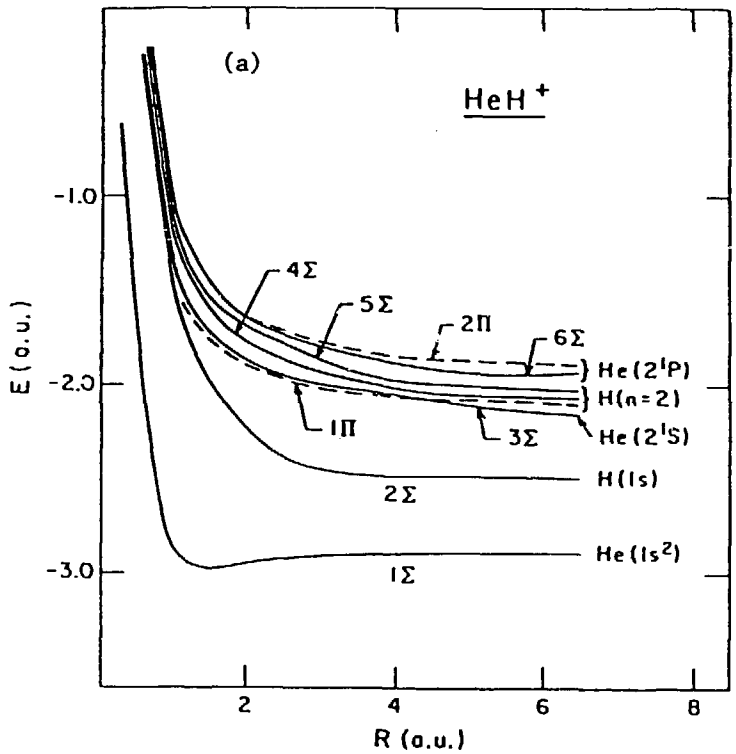

Fig. 12a. Collision of H^+ with He. Adiabatic potential curves.

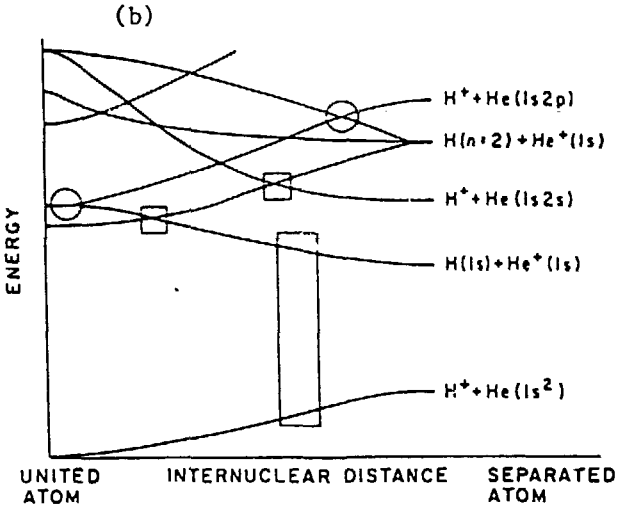

Fig. 12b. Schematic diabatic correlation diagram.

The charge transfer to the H(2p) state must proceed through a radial coupling at R ≈ 2 a.u. between the ground state of $H^+ + He(1^1s)$ and the first charge transfer state of $H(1s) + He^+(1s)$. The radial coupling between 3Σ and 4Σ, the angular coupling between 2Σ and 1Π at small R, and the Stark mixing between H(2s) and H(2p) at large R all contribute to the determination of the scattering probability and the phase for the H(2p) state.[25] The mechanism is quite complicated compared to two examples discussed in previous sections despite the simplicity of the system.

The integral alignment results are summarized in Fig. 13 along with recent measurements of the Bielefeld group.[17] At lower energies, charge transfer excitation to the H(2p) state is expected to proceed through the two-step process via $1\Sigma \rightarrow 2\Sigma \rightarrow 4\Sigma/5\Sigma$, mainly through a series of radial couplings. However, as the energies increase, the $2\Sigma - 1\Pi$ rotational coupling takes over within a two-step process and produces the $H(2P_{\pm 1})$ state. This helps to explain the increasing trend in A_{20} for $E \gtrsim 2$ keV. This trend is in contrast with the alignment result for the H/He system shown in Fig. 6. In fact, in the

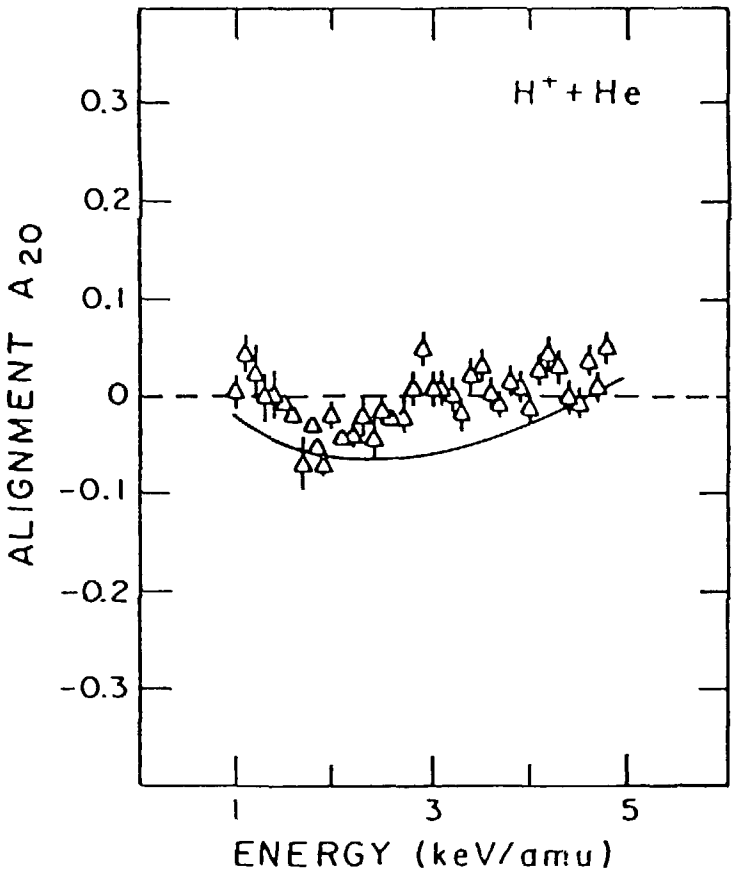

Fig. 13. Integral alignment for collision of H^+ with He. Curves are for calculated values (Ref. 23); Δ, experimental values (Ref. 17).

intermediate energy region ($1 \leq E \leq 20$ keV), the flux population process among excited and charge transfer states becomes extremely complex with respect to variations in energy and impact parameter; it may not be possible to single out a dominant mechanism. Although the coupling scheme among states remains complex, direct charge transfer to the excited state $H(2P_0)$ through a one-step process becomes increasingly important as the energy exceeds $E \sim 25$ keV. This mechanism is clearly reflected in the large negative values of A_{20}.

In Fig. 14, the orientation parameter is shown as a function of impact parameter/collision energy, along with the Bielefeld

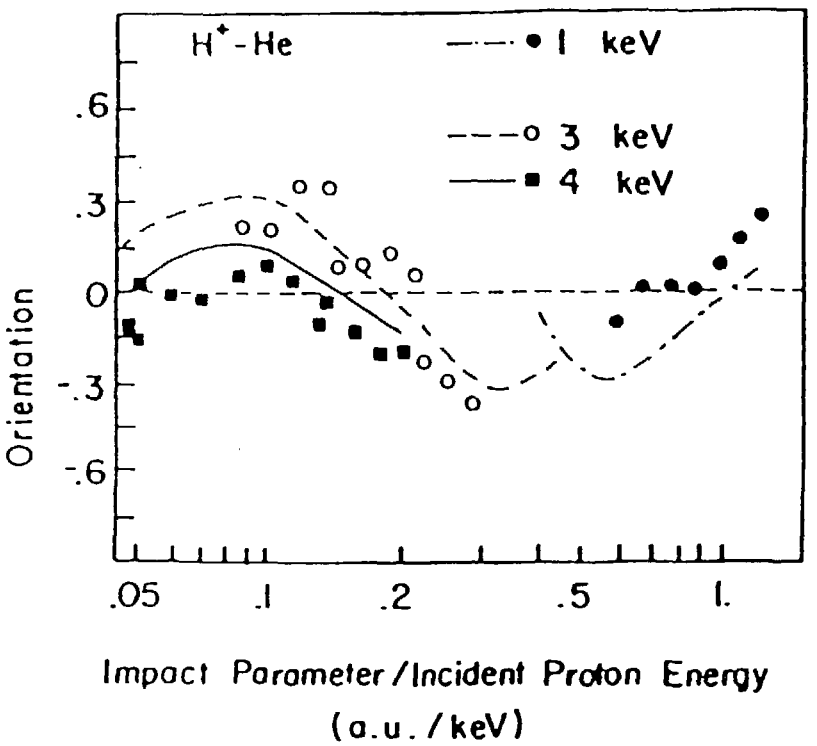

Fig. 14. Orientation parameter vs. impact parameter/collision energy for collision of H^+ with He. Symbols are experimental values (Ref. 17).

measurement.[17] As was seen in the integral alignment in Fig. 13, the $H(2P_0)$ and $H(2P_{\pm 1})$ cross sections are relatively sensitive both to impact parameter and energy in the energy region from 1 keV to 20 keV. Hence, the oscillatory behavior consistently observed both in the theory and the experiment is due to variations of both the magnitude of scattering amplitudes and the relative phase χ between the amplitudes a_{+1} and a_0 [see Eq. (8b)]. These two variations interrelate in a complicated manner to generate the oscillatory structure seen in Fig. 14. The inability of theory to reproduce these charac-

teristics in the alignment and orientation parameters within the context of a one-electron model[26] suggests that an explicit two-electron description, like that presented here, is essential to accurately determine these collision parameters.

As an example of the density matrix analysis, Fig. 15 compares the experimental dipole moment[4-6] of the H(n=3) excited state resulting from the charge transfer process in H^+ + He collisions with the theoretical value calculated by using the atomic orbital expansion method.[24] The large positive value of the dipole moment in the energy range 40-80 keV indicates that the center of the electron cloud distribution lags behind the projectile, being pulled toward the projectile from the target and lying between the two heavy particles at all energies.

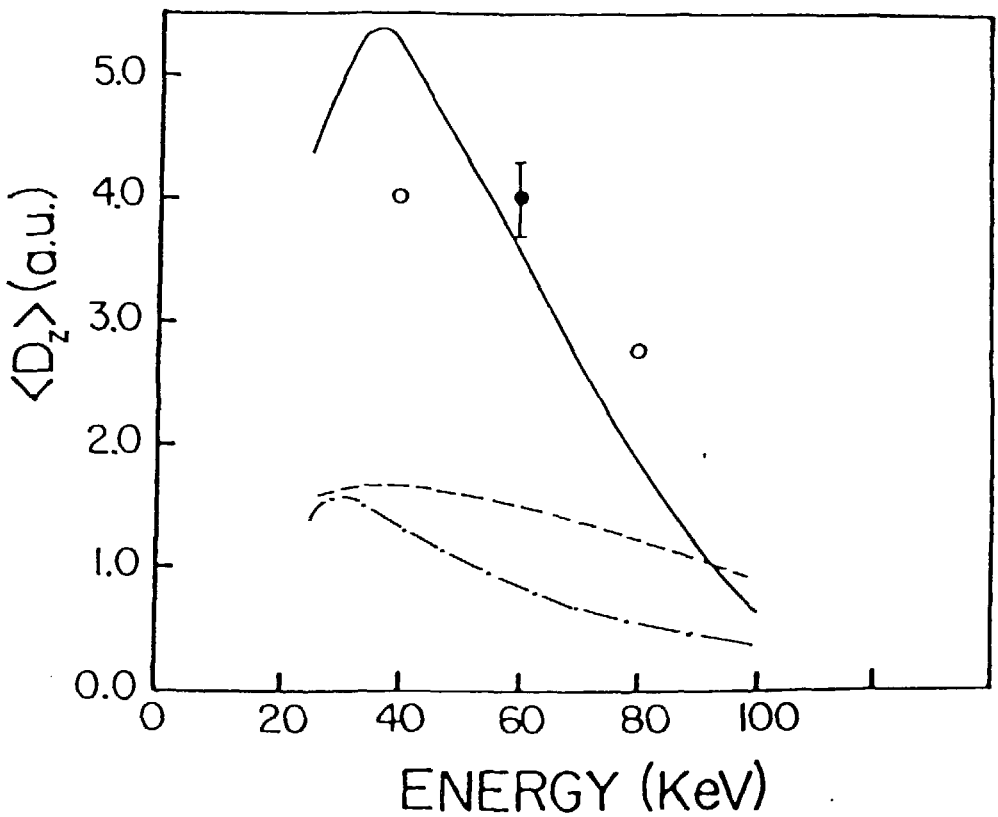

Fig. 15. Dipole moment of the H(n=3) excited state in collision of H^+ with He. Curves are calculated results (Ref. 24); symbols are experimental results (Refs. 4-6).

6. SUMMARY

We have attempted to illustrate recent progress in the theoretical study of alignment and orientation in ion-atom and atom-atom collisions at intermediate energies and to show how these parameters provide deeper insights into our understanding of the collision dynamics for various inelastic events. We have also provided illustration of the notion that a more elegant and complete way to elucidate the collision dynamics in ion-atom collisions is to determine the full density matrix for certain excited final states in a collision system. Further studies using the full density matrix for a variety of collision systems promise to provide better insights into atomic collision dynamics in general.

ACKNOWLEDGEMENTS

This work was supported in part by the U.S. Department of Energy, Office of Health and Environmental Research, under contract W-31-109-Eng-38 (MK), and the Office of Basic Energy Sciences, Division of Chemical Sciences, and Robert A. Welch Foundation (NFL).

References

1. Hippler, R. Electronic and Atomic Collisions (North Holland, 1988).
2. Hertel, I. V., Schmidt, H., Bähring, A., and Meyer. E. Rep. Prog. Phys. 48, 375 (1985).
3. Andersen, N., Gallagher, J. W., and Hertel, I. V. Electronic and Atomic Collisions (North Holland, 1986) p. 57.
4. Havener, C. C., Westerveld, W. B., Risley, J. S., Tolk, N. H., and Tully, J. C. Phys. Rev. Lett. 48, 926 (1982).
5. Havener, C. C., Rovz, N., Westerveld, W. B., and Risley, J. S. Phys. Rev. Lett. 53, 1049 (1984); Phys. Rev. A 33, 276 (1986).
6. Brower, M. C. and Pipkin, F. M. Bull. Am. Phys. Soc. 29, 816 (1984).
7. Kimura, M. and Lane, N. F. Phys. Rev. Lett. 52, 2160 (1986).
8. McDowell, M. R. C. and Coleman, J. P. Introduction to the Theory of Ion-Atom Collisions (North Holland, 1970).
9. Kimura, M. Electronic and Atomic Collisions (North Holland, 1986) p. 431.
10. Szasz, L. Pseudopotential Theory of Atoms and Molecules (Wiley Interscience, 1985).
11. Delos, J. B. Rev. Mod. Phys. 53, 287 (1981).
12. Kimura, M. and Thorson, W. R. Phys. Rev. A 24, 1780 (1981).
13. Fano, U. Phys. Rev. 90, 577 (1953).
14. Blum, K. and Kleinpoppen, H. Phys. Rep. 52, 204 (1979).
15. Winter, T. G., Dutta, C. M., and Lane, N. F. Phys. Rev. A 31, 2702 (1985).
16. Kimura, M. and Lane, N. f. Phys. Rev. A, in press.
17. Hippler, R, Harbich, W., Faust, M., Kleinpoppen, H., and Lutz, H. O. Proceedings of Tenth International Conference of Atomic Physics (1986) p. 485.
18. Kimura, M. and Lane, N. F. Unpublished results.
19. Andersen, T., Neitzke, P., Kimura, M. and Lane, N. F. J. Phys. B 20, 1789 (1987).
20. Wahnon, P., Gala, S., Diro, M. C., Caurbin-Gaussorgues, C., and Sidis, V. J. Phys. B 19, 611 (1986).

21. Andersen, N., Andersen, T., Neitzke, P., and Horsdal Pedersen, E. J. Phys. B 18, 2247 (1985).

22. Sidis, V., Stolterfoht, N., and Barat, M. J. Phys. B 14, 2815 (1977).

23. Kimura, M. and Lin, C. D. Unpublished results.

24. Jain, A., Lin, C. D., and Fritsch, W. Phys. Rev. A 35, 3180 (1987).

25. Kimura, M. Phys. Rev. A 31, 2153 (1985).

26. Fritsch, W. Private communication.